

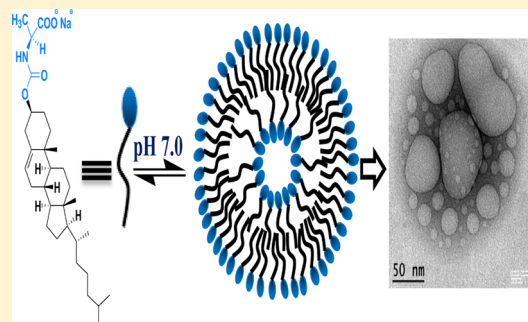
Spontaneously Formed Robust Steroidal Vesicles: Physicochemical Characterization and Interaction with HSA

Deepnath Bajani, Partha Laskar, and Joykrishna Dey*

Department of Chemistry, Indian Institute of Technology, Kharagpur – 721 302, West Bengal, India

S Supporting Information

ABSTRACT: Self-assembled multimolecular aggregates, such as vesicles, have earned tremendous attention for their applications as model membranes and drug delivery systems. Over the past decades, enormous efforts have been dedicated to the development of stable and biocompatible vesicles that form spontaneously in aqueous solution. With the aim of preparing highly stable vesicles, we herein report the physicochemical characterization of a novel cholesterol-based chiral surfactant with L-alanine headgroup. Different techniques, such as surface tensiometry, fluorescence spectroscopy, dynamic light scattering, UV–vis spectroscopy, transmission electron microscopy, and confocal fluorescence microscopy were employed to investigate the self-assembly properties of the aforementioned single-tailed steroidal surfactant in aqueous solution. The surfactant molecule is weakly surface-active, but self-assembles to form unilamellar vesicles facilitated by the strong hydrophobic association of the cholesterol moieties, above a very low critical aggregation concentration. The vesicles are fairly stable with respect to aging, temperature, and pH of the aqueous medium. Additionally, the vesicles were found to fuse together, leading to large unilamellar vesicles. The intervesicular fusion pertaining to high stability of the vesicles could be ascribed to large hydrophobic interactions among steroidal skeletons. Furthermore, the interaction of the vesicles with human serum albumin is also investigated.



INTRODUCTION

Molecular self-assembly and self-organization have been a fascinating research arena over the past decades.^{1–6} Small surfactant molecules capable of forming self-assemblies have long intrigued chemists for their wide applications. Especially, synthetic vesicles have gained the most attention not only for providing the fundamental insight on the self-assembly phenomena,^{7–11} but also for a myriad of applications in biomedicine, tissue engineering, gene therapy, and drug delivery.^{12–16} Vesicles are membrane-mimetic structures consisting of spherical bilayers of amphiphilic molecules (surfactants, lipids, or block copolymers), with an inner aqueous reservoir. Due to their bilayer structure, vesicles can encapsulate various materials, both hydrophobic and hydrophilic. Moreover, a vesicle can protect its cargo, i.e., a pharmaceutically active agent from the undesired enzymatic degradation until it reaches the site of interest. Additionally, the drug-loaded vesicles sequester the otherwise toxic effects associated with the high systemic concentration of the free drug.¹⁷ A stable vesicle endowed with sustained release profile enables high retention of the formulation in circulation and augmented drug availability at the site of action, thus reducing the effective dosage and the frequency of administration. Particularly, liposomes, which are phospholipid-derived vesicles, have been successfully used for the treatment of cancers, infectious and autoimmune diseases, as well as ocular inflammation.^{18–22} However, as far as stability is concerned,

liposomes have low storage life;²³ usually mechanical energy is required to disperse lipids in water. On the other hand, robust vesicles have been also made from amphiphilic polymers.²⁴ However, polymer vesicles are not promising in membrane fusion because the entanglement of polymeric chains in the microdomain structure markedly diminishes the membrane fluidity. Therefore, it is a huge challenge to seek a robust vesicle with ample membrane permeability. Also in designing a drug delivery system (DDS), one major issue that must be addressed is biocompatibility.

Steroids are widespread natural products with a tetracyclic ring system. Cholesterol (Chol) and bile acids typify the structural motif characteristic of steroids. Chol is an essential structural and functional component of animal cell membrane, whereby it modulates membrane fluidity and permeability.^{25–27} Additionally, Chol functions as a precursor for the biosyntheses of steroid hormones, bile acids, and vitamin D.²⁸ Within the cell membrane, Chol is also associated with many membrane-related bioprocesses, such as intracellular transport, signal transduction, and cell trafficking.^{29–31} Alteration of Chol profile leads to various diseases like gallstones, atherosclerosis, and myocardial infarction.³² However, thanks to its easy synthetic accessibility, tunability, chirality, nonimmunogenicity, and low

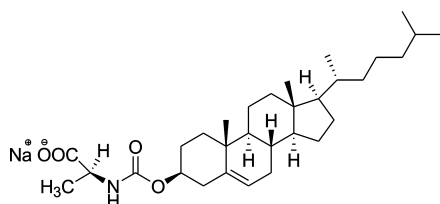
Received: January 11, 2014

Revised: April 5, 2014

Published: April 7, 2014

cost, Chol has turned out to be a fascinating building block for designing a variety of biologically relevant materials.³³ As already mentioned, Chol enhances the membrane rigidity thereby maintaining the ordered bilayer structure.³⁴ This invariably poses a question: Can Chol-based amphiphiles themselves self-assemble into bilayer structure? In fact, self-assembly of Chol-based amphiphiles has been investigated, mostly in terms of gelation.^{35,36} To date, reports on vesicle formation by Chol-based amino acid containing anionic surfactants are sparse.^{37–43} Therefore, we have designed a novel Chol-based single-tailed anionic surfactant, sodium *N*-(cholesterylformyl)-*L*-alaninate (NaChol-Ala, Chart 1), bearing

Chart 1. Chemical Structure of NaChol-Ala



L-alanine as the amino acid headgroup. Incorporation of biologically important molecules (e.g., Chol and amino acid in this case) could be a rule of thumb to improve the biocompatibility. Usually, double-tailed surfactants are well-known to form stable vesicles.⁴⁴ However, there are reports on vesicle formation by a mixture of two surfactants,^{45–47} and quite occasionally, by single-chain surfactants.^{48,49} Herein, we report stable vesicle formation by NaChol-Ala, a Chol-based single-tailed anionic surfactant with *L*-alanine as headgroup in aqueous buffered solution above a very low critical concentration. The tetracyclic steroidal nucleus of Chol can act as the hydrophobic domain-forming moiety and the amino acid as the polar headgroup.

Similar to Chol, bile salts also comprise a rigid tetracyclic steroidal nucleus connected to an aliphatic chain, and their physicochemical properties in aqueous solution are well-known.⁵⁰ At lower concentrations, bile salts form primary aggregates as micelles (with aggregation number <10 and approximate size in the range 10–16 Å) due to the back-to-back hydrophobic interactions between steroidal backbones, while larger elongated secondary micelles (size ~100 Å) are formed through hydrogen bonding association between the hydroxyl groups at increased concentrations. Structurally, bile salts have two (sodium deoxycholate, NaDC; sodium chenodeoxycholate, NaCDC) or three (sodium cholate, NaC; sodium taurocholate, NaTC) hydroxyl (–OH) groups in the steroidal moiety. Furthermore, unlike Chol having a nonpolar hydrocarbon chain, the aliphatic side chain in bile salts terminates with a polar group, usually carboxylates (NaC, NaDC, NaCDC) and sulfonates (NaTC). Thus, bile salts have a concave hydrophilic surface with –OH groups hanging from it, and a convex hydrophobic surface formed by the steroidal skeleton. The free –OH groups and the polar end-group, together with the steroidal framework make bile salts amphiphilic in nature, and account for their unique aggregation behavior in water. Although several models have been proposed to explain the aggregation phenomena, the two-stage aggregation model proposed by Small et al.⁵¹ has gained wide acceptance. In contrast to bile salts, Chol has one –OH group in the steroidal moiety. However, in NaChol-Ala, the free –OH

group of Chol has been conjugated to *L*-alanine amino acid through a carbamate linkage, thus making the steroidal backbone devoid of free hydroxyl groups. We thought such structural differences between Chol and bile acids may result a different aggregation behavior of NaChol-Ala in aqueous solution. Therefore, the effect of the absence of functional groups in the central portion of the framework on the aggregation properties of the Chol-based amphiphile is of particular interest in this investigation. The self-assembly formation by NaChol-Ala was characterized by use of a number of techniques including surface tensiometry, fluorescence spectroscopy, dynamic light scattering, and microscopy. Further, we have also performed a qualitative study on the interaction of NaChol-Ala with human serum albumin (HSA).

EXPERIMENTAL SECTION

Materials. Cholesteryl chloroformate was purchased from Sigma-Aldrich (Bangalore, India) and was used without further purification. Analytical grade *L*-alanine, NaOH, NaHCO₃, NaHPO₄, Na₂HPO₄, and HCl were obtained from SRL (Mumbai, India) and were used directly from the bottle. Fluorescence probes, *N*-phenyl-1-naphthalamine (NPN), pyrene (Py), coumarin-153 (C153), calcein (Cal), and 1,6-diphenyl-1,3,5-hexatriene (DPH) were purchased from Sigma-Aldrich (Bangalore, India) and were purified by recrystallization. HSA was also procured from Sigma-Aldrich (Bangalore, India). Deuterated chloroform (CDCl₃) was used as a solvent for NMR spectra. Tetrahydrofuran (THF), *n*-hexane, methanol, and acetone were of good quality commercially available, and were dried and distilled following standard procedures before use. The surfactant employed in this work was synthesized in our laboratory following reported procedure in the literature.⁵² The details of synthetic procedure and spectroscopic data for chemical identification are given in the Supporting Information (SI).

Methods. General Instrumentation. ¹H NMR and ¹³C NMR spectra were recorded on Bruker SEM 200 NMR spectrometers using tetramethylsilane (TMS) as the internal standard. A PerkinElmer RX1 FTIR spectrometer was used for recording Fourier transform infrared (FT-IR) spectra. The optical rotation was measured on a JASCO 370 digital polarimeter. Melting point was determined using InstInd (Kolkata) melting point apparatus with open capillaries. The pH measurements were carried out with a digital pH meter (Model 111) using a glass electrode. Turbidity measurements employed a Shimadzu Model 1601 UV–vis spectrophotometer. The percentage transmittance (%T) of surfactant solutions was measured at 400 nm at different time intervals. Turbidity (τ) was calculated using the relation, $\tau = 100 - \%T$. Aqueous phosphate buffer was prepared from Milli-Q water (18.2 M Ω), and was used for the solution studies. All measurements were done at 25 °C unless otherwise mentioned.

Surface Tension (ST). ST measurements were carried out with a surface tensiometer (model 3S GBX, France) at 25 ± 0.1 °C following the Du Nuöy ring detachment method. Prior to use, a platinum–iridium ring was cleaned with ethanol–HCl (1:1 v/v) solution. A stock solution of NaChol-Ala (1.1 mM) was prepared in pH 7.0 phosphate-buffered saline (PBS; 20 mM). Aliquots were added to 10.0 mL of pH 7.0 PBS taken in a Teflon bowl, and ST (γ mN m^{–1}) was measured after 10–15 min of equilibration. For each concentration, measurements were performed twice to check the reproducibility of the results, and the mean value of γ was noted.

Steady-State Fluorescence Measurements. The steady-state fluorescence measurements were performed on either a SPEX Fluorolog 3 or a PerkinElmer LS-55 luminescence spectrometer equipped with a temperature-controlled cell holder. NPN, C153, and Py were used as fluorescence probes to investigate the polarity of the microenvironment of the self-assemblies. For studies with NPN, a saturated solution of the probe in pH 7.0 PBS (20 mM) was used to make stock solution of the surfactant (0.21 mM). An aliquot of the surfactant solution was diluted to 5 mL by use of the saturated NPN solution. NPN was excited at 340 nm, and the emission spectrum was recorded in the wavelength range of 350–600 nm. Each spectrum was blank-subtracted. The excitation and emission slit widths were both set at 5.0 nm, and the intensity was measured at the emission maximum. For studies using C153, a stock solution (1.2×10^{-4} M) of the probe was prepared in dry methanol. At first, 40 μ L of the C153 stock solution was micropipetted into a 5 mL volumetric flask (in order to attain C153 concentration of 1×10^{-6} M) and evaporated to dryness by a gentle stream of N_2 . A measured volume of stock surfactant solution (0.21 mM) was then added. The pH 7.0 PBS was added to make the volume correct up to 5 mL. The excitation wavelength of C153 was 420 nm, and the emission spectrum was scanned in the range 430–650 nm setting excitation/emission band widths at 5 nm/5 nm. Py probe studies started off with the preparation of a stock solution of Py (1.2×10^{-4} M) in dry acetone, and the sample solutions were prepared following the similar procedure as in the case of C153. For Py, samples were excited at 325 nm, and the fluorescence spectrum was recorded between 340 and 440 nm with 5 nm/2 nm slit widths. The fluorescence intensity of Py was measured at the wavelengths corresponding to the first (I_1 , 374 nm) and the third (I_3 , 384 nm) vibronic bands. All fluorescence measurements were performed at 25 °C.

Steady-State Fluorescence Anisotropy Measurements. A PerkinElmer LS-55 Luminescence spectrometer was used to measure the steady-state fluorescence anisotropy (r) of DPH in the presence of the added surfactant. The instrument was equipped with a polarization accessory that used the L-format instrumental configuration. The software supplied by the manufacturer automatically determines the r -value. A stock solution of DPH (3.4×10^{-4} M) was prepared in dry methanol. Aliquots of this stock solution were added to the surfactant solutions so that the final concentration of the probe was 1 μ M. The anisotropy measurements were carried out with varying surfactant concentrations at 25–70 °C. Before measurements started, the solution was equilibrated for 10 min at the required temperature. The excitation wavelength was set to 350 nm, and the emission intensity was followed at 450 nm. The excitation and emission slit widths were 2.5 nm and 4.0–8.0 nm, respectively. A 430 nm cutoff filter was placed in the emission beam to eliminate the effect of scattered radiation. For each measurement, the anisotropy value was recorded over an integration time of 10 s. Five readings were recorded for each sample, and the average was accepted as the r value.

Time-Resolved Fluorescence Measurements. Fluorescence lifetime of DPH probe was measured on Optical Building Blocks Corporation EasyLife instrument. The light source was a 380 nm diode laser. The time-resolved decay curves were analyzed by single exponential or biexponential iterative fitting program. The best fit was judged by the χ^2 value (0.8–1.2) and the residual plot.

Determination of Microviscosity. The rigidity of the microenvironments of the self-assemblies was expressed in terms of microviscosity (η_m) experienced by DPH probe. In brief, η_m was calculated using the Stokes–Einstein–Debye equation:⁵³

$$\eta_m = \frac{k_B T \tau_r}{\nu_h} \quad (1)$$

where ν_h and τ_r are the hydrodynamic volume (313 \AA^3 for DPH probe molecule)⁵⁴ and rotational correlation time of the fluorophore, respectively. The τ_r value of DPH in the surfactant solution was estimated from Perrin's equation:⁵⁵

$$\tau_r = \frac{\tau_f}{\left(\frac{r_0}{r} - 1\right)} \quad (2)$$

where r_0 ($= 0.362$)⁵⁶ and r are the steady-state fluorescence anisotropy values of the DPH probe in a highly viscous solvent and in sample, respectively; τ_f is the measured average fluorescence lifetime of DPH in the surfactant solution.

Dynamic Light Scattering (DLS) and Zeta Potential. The DLS technique was used to measure the size distribution of the aggregates formed in aqueous solution. The DLS measurements employed a Zetasizer Nano ZS (Malvern Instrument Lab., Malvern, U.K.) light scattering spectrometer equipped with a He–Ne laser working at 4 mW ($\lambda_0 = 632.8$ nm). The sample solutions were filtered directly into the scattering cell through a Millipore Millex syringe filter (Triton-free, 0.22 μ m). Each sample was allowed to equilibrate inside the DLS optical system chamber for 10 min prior to the start of the measurement. All measurements were performed at 25 ± 0.1 °C. The scattering intensity was measured at 173° to the incident beam. At least 12 runs were performed for each sample. The software supplied by the manufacturer automatically calculates the optimum parameters for monomodal as well as for multimodal distributions in order to produce a size distribution profile. Zeta (ζ) potential measurements were also performed on the same instrument.

Transmission Electron Microscopy (TEM). The morphology of the aggregates was visualized by a transmission electron microscope (FEI-TECNAI G2 20S-TWIN, FEI, USA) operating at an accelerating voltage of 120 kV. TEM pictures were taken for 0.06 and 0.12 mM surfactant solutions in pH 7.0 PBS (20 mM). A 5 μ L volume of surfactant solution was dropped on to a 400 mesh size carbon-coated copper grid, and allowed to stand for 1 min. The excess solution was blotted with a piece of tissue paper, and the grid was air-dried. The specimens were kept in desiccators overnight before measurement. Each measurement was repeated at least twice to check the reproducibility.

Confocal Fluorescence Microscopy (CFM). The optical microscopic images of Cal-trapped vesicles were recorded by Olympus FluoView FV1000 confocal fluorescent microscope that used a 488 nm laser source. For entrapment of Cal, NaChol-Ala (0.31 mg, 0.59 mmol) and Cal (208 μ L, 0.48 mM) in methanol (5 mL) were taken in a 25 mL RB flask, and homogenized by sonication. Next, methanol was evaporated in a rotavapor, and the mixture was dried thoroughly in vacuum desiccators. The resulting thin film was soaked with 500 μ L of PBS (pH 7.0, 20 mM) overnight, and then diluted to 5 mL such that the final concentrations of the surfactant and Cal were 0.12 mM and 2×10^{-5} M, respectively. The excess dye was removed by dialysis for 2 h, using an ultrafiltration cellulose

acetate membrane with pore size of 1000 Da MWCO. A few microliters of the dialyzed solution was poured onto a glass slide which was then sealed with a coverslip and placed in the microscope.

RESULTS AND DISCUSSION

Interfacial Properties. The surface activity of NaChol-Ala was studied in pH 7.0 PBS (20 mM) at 25 °C. Figure 1 depicts

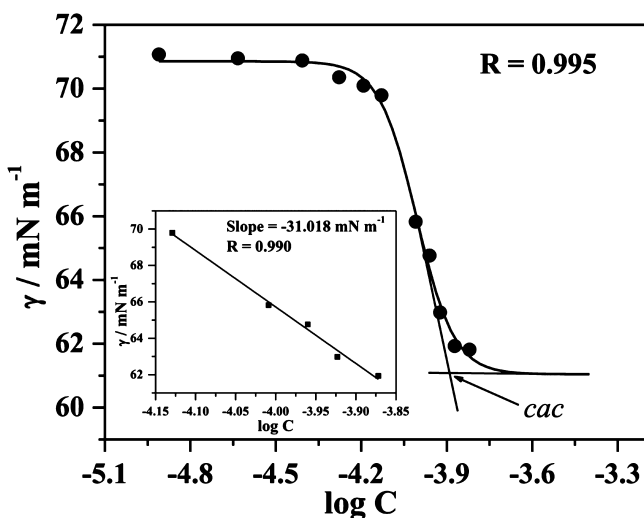


Figure 1. Plot showing the variation of γ (mN m^{-1}) with $\log C$ at 25 °C; inset showing linear fitting of the γ versus $\log C$ plot.

the surface tension (γ) versus \log [NaChol-Ala] plot. The ST value attained its minimum of 62 mN m^{-1} at a concentration of ca. 0.13 mM of NaChol-Ala. This suggests that the surfactant under study is weakly surface-active in comparison to common anionic surfactants like sodium *N*-(11-acrylamidoundecanoyl)-*L*-alaninate (SAUA; critical aggregation concentration (cac) 0.22 mM, $\gamma_{cac} 52.3 \text{ mN m}^{-1}$)⁵⁷ and bile salt, NaDC (cac 3.7 mM, $\gamma_{cac} 44.8 \text{ mN m}^{-1}$)⁵⁸, where cac is the critical aggregation concentration and γ_{cac} is the surface tension at cac . The surfactant concentration (0.13 mM) corresponding to the minimum value of γ can be taken as the cac . Thus, the cac value is much less than those of SAUA and NaDC. Furthermore, the saturation adsorption (Γ_{max}) was calculated from the slope of the linear part of γ versus $\log C$ plot (inset of Figure 1) using Gibbs adsorption equation:⁵⁹

$$\Gamma_{max} = -\frac{1}{2.303nRT} \frac{d\gamma}{d \log C} \quad (3)$$

where C is the concentration of the surfactant, N_A is Avogadro constant, R is the gas constant, T is the temperature in Kelvin, and $n = 2$ for dilute solutions of 1:1 ionic surfactant.⁵⁹ The minimum surface area per surfactant molecule ($A_{min} = 62 \text{ \AA}^2$) and molecular packing parameter (P) was calculated using the equations:⁶⁰

$$A_{min} = \frac{1}{\Gamma_{max}} N_A \quad (4)$$

and

$$P = \frac{\nu}{l_c A_{min}} \quad (5)$$

where ν and l_c are respectively the volume and extended chain length of the hydrophobic tail. The molecular volume (ν) of Chol was calculated from its molar volume ($391.4 \pm 5.0 \text{ cm}^3 \text{ mol}^{-1}$).⁶¹ On the other hand, l_c (17.15 Å) was determined by energy minimization of the surfactant structure using MM2 force field in Chem3D Ultra 7.0 software (Cambridge Soft Corporation). The P value of 0.61 thus obtained indicates the formation of bilayer vesicles.⁶⁰

Fluorescence Probe Studies. Fluorescence probe analysis is an important area in biophysical studies of molecular assemblies, such as micelles, vesicles etc. Using extrinsic fluorescent probes, the self-aggregation phenomena along with the nature of the microenvironment (particularly, micropolarity and microviscosity) can be addressed. In the present study, we used NPN, C153, and Py as polarity probes and DPH as the viscosity probe. The hydrophobic probe molecules have poor solubilities in water, but they become solubilized in the nonpolar microdomain of the self-assemblies formed by the surfactant molecules. Thus, the fluorescence profiles of these probes in the absence and the presence of the surfactant can throw light on the aggregation phenomena.

Studies with NPN Probe. NPN has been successfully employed as a polarity probe, since its fluorescence emission spectrum exhibits a large blue shift with a concomitant enhancement in fluorescence intensity on moving from a polar to a nonpolar environment.⁶² In the present study, the fluorescence emission spectrum of NPN was recorded in the absence and the presence of NaChol-Ala (see Figure S4 of the SI). In aqueous buffer (pH 7.0 PBS), NPN exhibited a very weak fluorescence with emission maximum (λ_{max}) centered at ~455 nm. A large blue shift (~40 nm) of the emission maximum accompanied by ca. 6-fold increase of fluorescence intensity was observed in the presence of NaChol-Ala (0.12 mM). This clearly suggests that the probe molecules are solubilized within the hydrophobic microdomain formed by

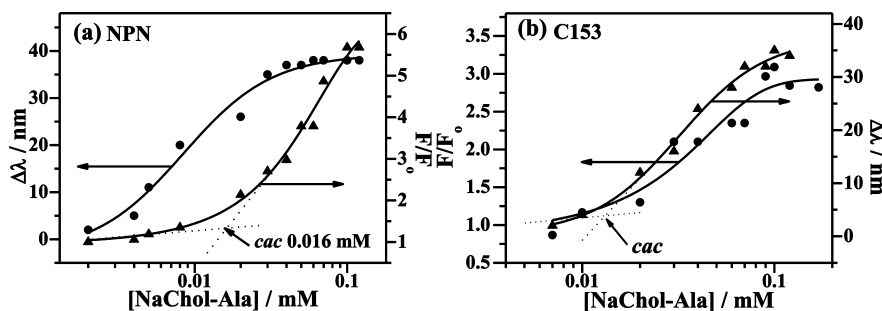


Figure 2. Variation of relative fluorescence intensity (F/F_0) and spectral shift ($\Delta\lambda$) of (a) NPN and (b) C153 as a function of [NaChol-Ala] at 25 °C.

self-aggregation of the surfactant molecules. Figure 2a shows the variation of relative fluorescence intensity (F/F_0) and spectral shift ($\Delta\lambda = \lambda_{\max(\text{buffer})} - \lambda_{\max(\text{sample})}$) of NPN as a function of [NaChol-Ala], where F_0 and F are the fluorescence intensities in the absence and the presence of the surfactant, respectively. Each of the fluorescence titration curves was fitted to sigmoidal growth function corresponding to a two-state process. The best fit was judged by the R value (~ 0.985). It is evident from the intensity profile that below a critical concentration (c_{ac}) equal to ca. 0.016 mM, there are no aggregates present, and the NPN spectrum corresponds to that in buffer. However, as the surfactant concentration rises above 0.016 mM, more and more probe molecules are solubilized within the hydrophobic interior, as can be rationalized from the sigmoidal growth terminating with a plateau. The inflection point corresponding to a concentration of ca. 0.016 mM indicates the onset of aggregation phenomenon, and therefore, can be taken as the c_{ac} value. However, the c_{ac} value as obtained from fluorescence titration is one-order of magnitude less than that obtained from ST plot. This might be due to weak surface-activity of the surfactant, which results in small changes in γ -value with the increase of [surfactant]. Since fluorescence is a more sensitive technique than ST, the c_{ac} value obtained from the fluorescence titration curve was taken to be more accurate.

Studies Using C153 Probe. C153 has been extensively used as a solvation dynamics probe.⁶³ Like NPN studies, we again found a large blue shift of the fluorescence spectrum of C153 along with an increase in intensity in the presence of surfactant (see Figure S5, SI). The c_{ac} value obtained from the F/F_0 versus [NaChol-Ala] plot (Figure 2b) is in good agreement with the results obtained from NPN studies. Here also, a good fit ($R = 0.94, 0.99$) of the plots with sigmoidal growth function was observed suggesting a two-state process. The c_{ac} value obtained from the inflection point is ca. 0.015 mM, which is closely similar to the value obtained from fluorometric titration using NPN and confirms accuracy of the measurements. In addition to providing a quantitative measure of the c_{ac} , the solvatochromic character of C153 affords a very good correlation between solvent polarity and emission frequency of C153. The micropolarity of the self-assemblies can be usually expressed in terms of π^* solvent polarity scale, which is given by the relation⁶⁴

$$\bar{\nu}_{em} = 21.217 - 3.505\pi^* \quad (6)$$

where $\bar{\nu}_{em}$ [in 10^3 cm^{-1}] is the frequency corresponding to the limiting emission maximum of C153 in the presence of surfactant. In our case, the π^* value of ~ 0.50 in the presence of 0.12 mM NaChol-Ala suggests that the polarity of the microenvironment is comparable with that of 2-propanol ($\pi^* = 0.49$).⁶⁴ The experimental results are summarized in Table S1 (SI).

Studies with Pyrene Probe. Studies with Py as a fluorescent probe have earned significant consideration in the area of molecular self-assembly. Py is a strongly hydrophobic probe having poor water solubility (2–3 μM). The relative fluorescence intensities of the various vibronic bands of Py monomer show strong dependence on the solvent environment around it.⁶⁵ Several mechanisms underlying the interactions of the excited states of Py molecules with surrounding solvent molecules have been discussed in the literature.⁶⁶ However, the solvent-dependent perturbation of the vibronic band intensities has been used to determine the micropolarity and the extent of

water penetration into micellar and membrane-like microdomains.⁶⁵ In particular, the intensity ratio of the first (I_1 , 374 nm) to the third (I_3 , 384 nm) vibronic band in the Py fluorescence spectrum is typically used as an index of the apparent micropolarity. The I_1/I_3 ratio is, thus, often termed the “polarity ratio”. The fluorescence emission spectra of Py measured in PBS buffer (pH 7.0) in the absence and the presence of different concentrations of NaChol-Ala are shown in Figure S6 of SI. Figure 3 presents the variation of the I_1/I_3

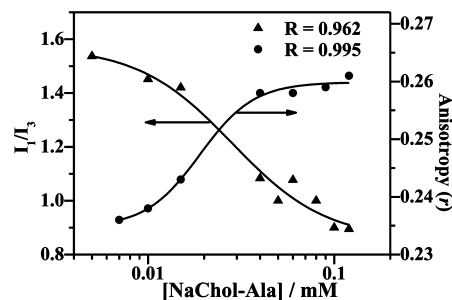


Figure 3. Variation of I_1/I_3 of Py and fluorescence anisotropy (r) of DPH probe as a function of [NaChol-Ala] at 25 °C.

ratio as a function of the surfactant concentration, and affords several interesting results. The plot fits best ($R = 0.962$) to a sigmoid function confirming a two-state process. The I_1/I_3 ratio has a value of 1.75 in pH 7.0 PBS (20 mM) in the absence of the surfactant. However, the ratio falls off with increasing concentration of the added surfactant, indicating the formation of aggregates with less polar local environment. The limiting steady value of I_1/I_3 is equal to 0.89. It is interesting to note that the I_1/I_3 values for bile salts, such as NaC (0.79),^{67,68} and NaDC (0.71)⁶⁷ are also very small and much lower than that of SAUA (1.30).⁵⁷ This suggests that the polarity of the microenvironment of the self-assemblies formed by NaChol-Ala is very low, and closely resembles that of 2-propanol. It is worth mentioning here that the C153 probe study also indicated a 2-propanol-like micropolarity, thus showing a great deal of reliability of the experimental findings.

Studies Using DPH Probe. Degree of depolarization of fluorescence emission is indicative of rotational diffusion of an excited fluorophore, and affords a means to probe the microenvironment of molecular self-assemblies and hence the shape of the aggregates. DPH is a membrane fluidity fluorescent probe and is widely used for studying lipid bilayer aggregates.^{69,70} The steady-state fluorescence anisotropy (r) value of DPH probe is an index of rigidity of the local environment of the interior core of the aggregates. Normal micelles of ionic surfactants have low anisotropy values of ~ 0.05 ,⁷¹ and vesicles have r values usually greater than 0.14. Figure 3 depicts the variation of anisotropy of DPH probe with surfactant concentration at 25 °C. It is observed that the r value increases steeply with [NaChol-Ala] above its c_{ac} value, and reaches a saturation plateau at $r = 0.26 \pm 0.01$ following a sigmoid function ($R = 0.995$). The high r value suggests that the probe is solubilized within the highly viscous microdomain, and is indicative of the formation of bilayer vesicles, which will be justified through further studies.

To determine the microviscosity (η_m) of the aggregates in aqueous solution, we performed time-resolved fluorescence lifetime measurements using DPH probe. The fluorescence lifetime (τ_f) of the DPH probe was measured in the presence of

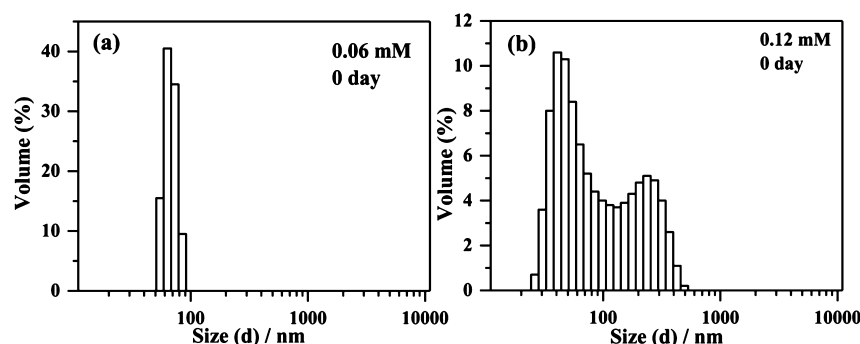


Figure 4. Size distribution histograms of surfactant solutions in pH 7.0 PBS (20 mM) at 25 °C for (a) 0.06 mM NaChol-Ala at $t = 0$ day, and (b) 0.12 mM NaChol-Ala at $t = 0$ day.

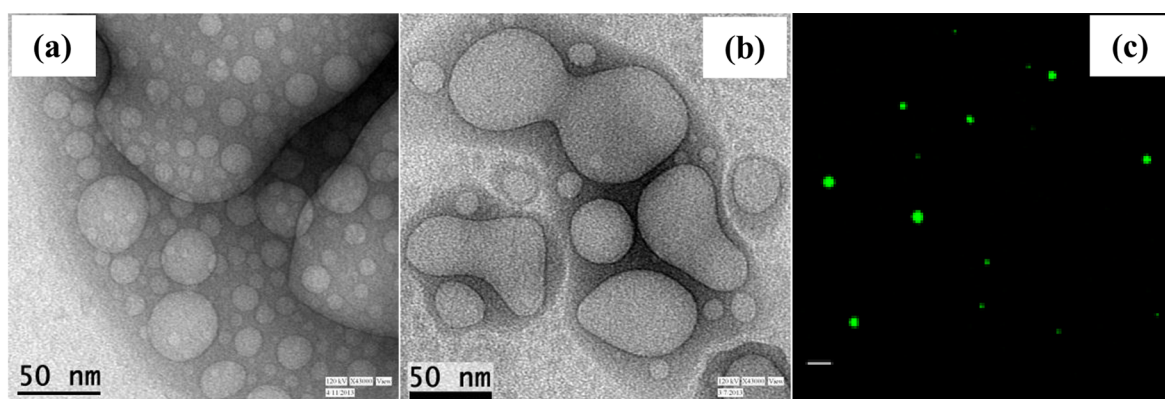


Figure 5. Unstained TEM images of the vesicles of (a) 0.06 mM and (b) 0.12 mM NaChol-Ala solution. (c) CFM image of the Cal-loaded vesicles (scale bar is 5 μm).

0.06 mM and 0.12 mM surfactant solutions in pH 7.0 PBS (20 mM). For both the concentrations, the experimental time-resolved intensity profile fits well to biexponential decay with χ^2 -values within the fairly accepted range. The time-resolved fluorescence data are listed in Table S2 of the SI. Major contribution ($\geq 94\%$) to τ_f value stems from only one of the components, which was used for the calculation of η_m . The experimental high τ_f values reflect that the probe molecules are partitioned into the hydrophobic environment of the self-assemblies. The η_m values (ca. 222 and 227 mPa s) thus obtained were much larger compared to micelle-forming DTAB, SDS, and Tx-100 surfactants.⁵⁴ Such high η_m values indicate very rigid and viscous microenvironment of the aggregates, which must be due to the tight packing of the cholesteryl moieties forming bilayers.

Hydrodynamic Size of Aggregates. DLS studies showed a monomodal (PDI = 0.756) size distribution around a mean hydrodynamic diameter (d_h) of 70–80 nm (Figure 4a) in the case of 0.06 mM NaChol-Ala solution in pH 7.0 PBS at 25 °C. However, with 0.12 mM NaChol-Ala, a bimodal (PDI = 0.324) size distribution with peaks at ~ 50 nm and ~ 250 nm (Figure 4b) was obtained. This indicates that unlike bile salts, NaChol-Ala forms large bilayer aggregates, probably vesicles, with relatively narrow size distribution. Although usually a broad size distribution is observed in dilute surfactant solution, in the present case, the higher PDI value in 0.06 mM solution could be due to the nongaussian feature of the distribution.

Microstructure of the Aggregates. *Transmission Electron Microscopy (TEM).* In order to gain a clear and foolproof insight into the size and shape of the self-assembled microstructures, TEM pictures were taken. Representative

TEM images are shown in Figure 5a,b. Both micrographs reveal the presence of small unilamellar vesicles (SUVs). A close look at the images shows that the vesicles are mostly spherical in shape, and the size ranges from 10 to 100 nm. However, as observed in Figure 5b, at higher surfactant concentration, the SUVs fuse together, leading to the formation of large unilamellar vesicles (LUVs) of diameter in the range 100–200 nm. This may be attributed to strong hydrophobic interactions arising from the Chol moieties. In addition to spherical vesicles, however, fewer elongated vesicles (50–80 nm) are also visible. The TEM images are consistent with the findings from DLS and fluorescence anisotropy studies that suggested the presence of highly rigid bilayer structures in aqueous buffered solutions.

Confocal Fluorescence Microscopy (CFM). Because TEM sample preparation procedure involves drying of the specimen, TEM micrographs are often criticized for generating artifacts. Although TEM images were reproducible, CFM was used to visualize the dye-entrapment within the aqueous core of the vesicles in support of the TEM results. We employed calcein (Cal) dye for this study. The CFM image presented in Figure 5c clearly shows the existence of spherical vesicles with aqueous core loaded with green fluorescent Cal. The vesicles have sizes in the range of 500 nm to 2 μm . It should be remembered that, in contrast to TEM, CFM cannot resolve vesicles smaller than 200 nm because of its limitation. Therefore, only larger vesicles that were formed by fusion of SUVs are observed. Thus, the CFM image presents a further proof of the presence of spherical vesicles.

Stability of the Vesicles. Once we confirmed the formation of unilamellar vesicles, the next challenge was to

investigate their stability with respect to aging, temperature, and pH of the aqueous solution. For that purpose, we measured zeta potential, turbidity, hydrodynamic size, and steady-state fluorescence anisotropy of the vesicular assemblies.

Zeta Potential. The ζ -potential is a measure of the degree of repulsion between adjacent, similarly charged particles in dispersion. A high ζ -potential value (positive or negative) is indicative of the system's stability against flocculation or coagulation. Low ζ -potential values (-5.5 mV and -8.9 mV for 0.06 and 0.12 mM NaChol-Ala, respectively) suggest that the dispersion tends to collapse leading to flocculation or coagulation. Relatively low ζ -values are expected for carboxylate surfactants as their salts hydrolyze in dilute solution to produce corresponding acid form, which reduces the intermolecular repulsion among surfactant molecules in the aggregates, thus allowing molecules pack tightly. However, the negative charge density being less, the vesicles are expected to be less stable because of weaker electrostatic repulsions among vesicles as discussed below.

Aging Effect. In order to investigate the stability of the vesicles, the turbidity ($\tau = 100 - \%T$) of the surfactant solution was measured at different time intervals. Basically, turbidity arises from the scattering of light by the dispersed vesicles, and depends on their sizes and populations. The turbidity of 0.06 mM and 0.12 mM surfactant solutions in pH 7.0 PBS (20 mM) buffer was measured at 400 nm at different time intervals during 25 days. The experimental results are presented in Figure 6. The plot reveals that the turbidity initially increases

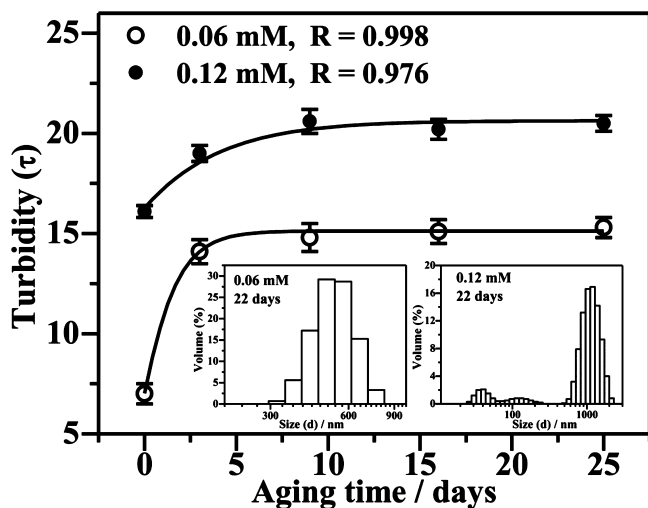


Figure 6. Effect of aging on the vesicular aggregates: Plot of turbidity versus aging time; inset shows size distribution histograms after 22 days for 0.06 mM and 0.12 mM NaChol-Ala.

only slightly with time for $[\text{NaChol-Ala}] = 0.06$ mM, and reaches almost a steady value. In the case of concentrated solution, turbidity remains almost constant throughout the aging period. The initial increase in turbidity in the case of 0.06 mM surfactant solution could be traced to the formation and growth of vesicles, while the subsequent plateau mirrors good storage life of the vesicles.

The effect of aging was further rationalized in terms of the time-variation of size distribution of the vesicles. As shown by the size distribution histograms in the inset of Figure 6, the mean value of d_h increased to ca. 530 nm for 0.06 mM (PDI = 0.482) and to ca. 1025 nm for 0.12 mM (PDI = 0.616)

surfactant solutions, respectively after 22 days. The explanation can be sought in terms of intervesicular fusion leading to the formation of larger vesicles (>500 nm) as shown in the TEM picture Figure 5(b). The PDI value for the 0.12 mM solution is also observed to increase with aging and is consistent with the appearance of a trimodal distribution profile. In contrast, for 0.06 mM solution, the PDI value is reduced to 0.482.

Thermal Stability. The thermal stability of the vesicles was investigated by measuring fluorescence anisotropy (r) of the DPH probe at various temperatures. Figure 7a represents the variation of r with increasing temperature for $[\text{NaChol-Ala}] = 0.06$ mM. The plot shows that the r value is quite high at room temperature, indicating the existence of bilayer vesicles. However, the r value decreases with the rise in temperature, but it lies in the vesicular range, even at 70 °C. This tells us that the bilayer membrane of vesicular aggregates becomes less rigid at elevated temperatures as an outcome of weakening of the packing of the Chol units due to gel-to-liquid crystalline phase transition. The weak packing of the Chol units also results in water penetration, thus causing hydration of the bilayer membrane. Such phenomenon has also been reported earlier by others in the case of Chol-containing niosomes.^{72,73} The phase transition temperature T_m as obtained from the inflection point of the plot is ca. 46 °C, which is higher than the physiological temperature (37 °C). Because the vesicles are stable at the physiological temperature, they are expected to have good lifetime in the blood circulation, unless they bind serum proteins strongly.

Dye Entrapment and pH Stability. The surfactant under study has a COO^- headgroup which can be protonated in pH below its pK_a value. On the other hand, the surfactant has a carbamate linkage ($-\text{O}-(\text{C}=\text{O})-\text{NH}$) connecting the Chol unit with the amino acid headgroup. The carbamate bond is susceptible to hydrolysis at low pH, thus making the vesicle structure unstable. Further, it is known that different tissues of biological system and biofluids (e.g., blood, tear, saliva, urine, gastric juice, etc.) have pH in the range of 2.0 to 8.⁷⁴ Therefore, to test whether the vesicles were stable at acidic pH, we encapsulated DPH (1 μM) within the hydrophobic membrane, and monitored its release at bulk pH of 7.4 and ~ 4.5 at 37 °C. Because DPH has negligible water solubility, there must be a decrease in fluorescence intensity when the vesicles are disrupted, resulting in release of DPH molecules to bulk water. To a 5 mL of DPH-trapped NaChol-Ala solution (0.12 mM) in pH 7.4 PBS, 245 μL of HCl (pH 0.60) was added to attain a bulk pH of 4.5. The addition of HCl was taken to be done at $t = 0$. The fluorescence intensity of DPH was measured at different time intervals. The % release was calculated from the value of $(1 - F/F_\infty) \times 100\%$, where F and F_∞ are the fluorescence intensities of DPH at any time t and at the end of the 2 h time period, respectively. Notably, only $\sim 5\%$ of encapsulated DPH probe was released in 2 h in pH ~ 4.5 (see Figure 7b). This shows that the vesicles are stable enough even at acidic pH and could serve as a system for sustained release of hydrophobic drugs.

Interactions with HSA. HSA is the most abundant protein in human blood and is responsible for the transport of various metabolites, fatty acids, and drug molecules.^{75,76} It is a globular protein with a single tryptophan (Trp214) residue. The interaction of HSA with a DDS (particularly injectable) is important in the viewpoint of the lifetime of the latter in the circulation. To investigate the fate of the vesicular assemblies in the circulation, we have studied the interaction of HSA with the

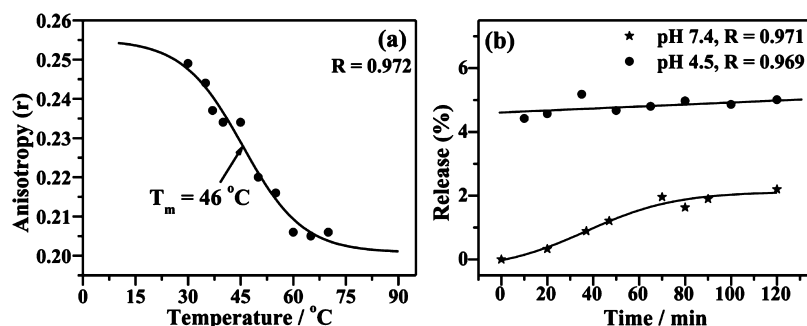


Figure 7. (a) Plot showing thermal stability of the vesicles. (b) Release profile of DPH encapsulated in the vesicles in pH 7.4 and 4.5 at 37 °C.

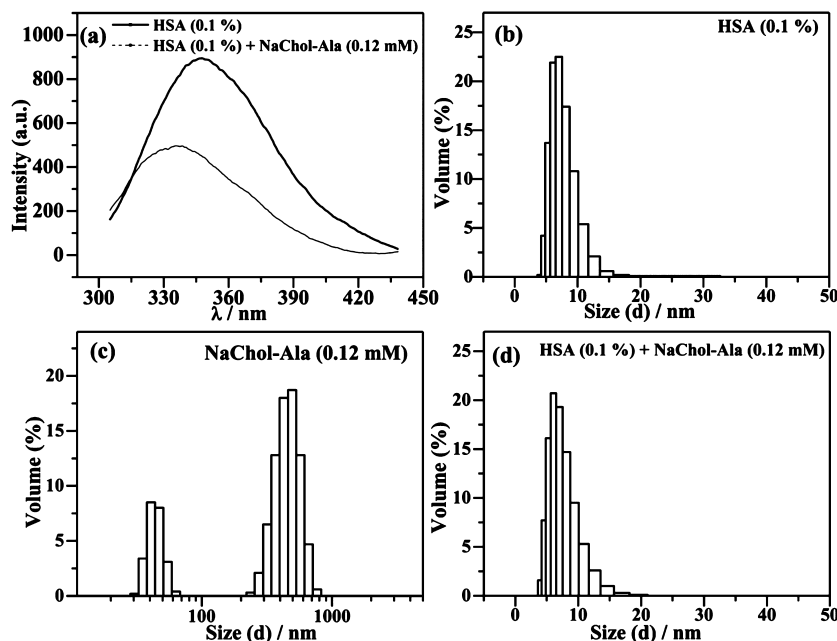


Figure 8. (a) Fluorescence intensity profile of HSA in the absence and presence of NaChol-Ala; Size distribution profiles after 24 h incubation: (b) HSA (0.1%), (c) NaChol-Ala (0.12 mM), and (d) HSA (0.1%) + NaChol-Ala (0.12 mM).

vesicles after a 24 h incubation period at room temperature. When excited at 295 nm, the protein (0.1% w/v) alone showed its emission maximum around 348 nm in pH 7.0 PBS (20 mM), but in the presence of 0.12 mM NaChol-Ala, we observed a 13 nm blue shift in the emission maximum as well as a quenching of the Trp fluorescence (Figure 8a). This suggests binding of the vesicles with HSA. In the presence of NaChol-Ala, the Trp214 experienced a more hydrophobic region, which may be attributed to the presence of hydrophobic Chol moieties. In fact, the binding of bile salts to HSA and BSA are also known to occur through hydrophobic interactions.^{77,78} This means NaChol-Ala binds to hydrophobic pocket of HSA near Trp214. To be sure of it, we further performed DLS measurements with the protein (0.1%) in the absence and presence of NaChol-Ala. Figure 8b–d clearly show that the distribution corresponding to vesicular aggregates completely vanishes in the presence of protein which means disruption of vesicles. Therefore, it can be concluded that despite small size and sufficient stability such vesicles cannot be employed as injectable DDS.

CONCLUSIONS

In conclusion, we have designed and synthesized a new carboxylate surfactant with Chol as hydrophobic tail. The

physicochemical and self-assembly properties of the amino acid-derived steroidal surfactant, NaChol-Ala, have been reported. Unlike conventional fatty acid surfactants with hydrocarbon tail or bile salts, the amphiphile showed weak surface activity. In fact, the surface-activity of NaChol-Ala is much weaker than NaDC or NaC. We have investigated the intriguing self-assembly properties of the surfactant. Unlike bile salts, NaChol-Ala is shown to form small (50–250 nm) and stable unilamellar vesicles in neutral as well as in slightly acidic pH. The vesicles were also observed to be sufficiently stable at physiological temperature for a longer period of time. The driving force for vesicle formation is the large hydrophobic interactions between Chol blocks leading to compact packing, which makes the vesicles stable and robust. The vesicular aggregates may find applications in sustained drug delivery. Since the vesicles bind to HSA strongly, without the incorporation of further stabilizing agent (for example, poly(ethylene glycol)), they may not be useful as injectable drug delivery system. However, their tendency to form larger aggregates on standing can offer them potential for dermal delivery of antibacterial agents, sunscreens, or cosmetics. Work on Chol-derived surfactants bearing other amino acids is currently underway in this laboratory.

■ ASSOCIATED CONTENT

■ Supporting Information

Details of synthetic procedure, FT-IR, ¹H NMR, and ¹³C NMR spectra and chemical identification of the synthesized amphiphile, representative fluorescence emission spectra of NPN, C153, and Py are available free of charge via the Internet at <http://pubs.acs.org>.

■ AUTHOR INFORMATION

Corresponding Author

*Fax: (+) 91-3222-255303; E-mail: joydey@chem.iitkgp.ernet.in.

Notes

The authors declare no competing financial interest.

■ ACKNOWLEDGMENTS

The authors thank the Indian Institute of Technology, Kharagpur, for financial support of this work. P.L. acknowledges CSIR, India, for research fellowships. We are thankful to Prof. N. Sarkar for the DLS and zeta potential measurements and Mr. B. Roy for his help with the fluorescence microscopic measurements.

■ REFERENCES

- (1) Whitesides, G. M.; Grzybowski, B. Self-Assembly at All Scales. *Science* **2002**, *295*, 2418–2421.
- (2) Lehn, J.-M. Toward Self-Organization and Complex Matter. *Science* **2002**, *295*, 2400–2403.
- (3) Brizard, A.; Stuart, M.; Bommel, K. V.; Friggeri, A.; Jong, M. D.; Esch, J. V. Preparation of Nanostructures by Orthogonal Self-Assembly of Hydrogelators and Surfactants. *Angew. Chem., Int. Ed.* **2008**, *47*, 2063–2066.
- (4) Verma, G.; Hassan, P. A. Self-assembled Materials: Design Strategies and Drug Delivery Perspectives. *Phys. Chem. Chem. Phys.* **2013**, *15*, 17016–17028.
- (5) Mai, Y.; Eisenberg, A. Self-assembly of Block Copolymers. *Chem. Soc. Rev.* **2012**, *41*, 5969–5985.
- (6) Kato, T.; Mizoshita, M.; Kishimoto, K. Functional Liquid-Crystalline Assemblies: Self-Organized Soft Materials. *Angew. Chem., Int. Ed.* **2006**, *45*, 38–68.
- (7) Israelachvili, J. N. *Intermolecular and Surface Forces*, 2nd ed.; Academic Press: New York, 1992.
- (8) Guida, V. Thermodynamics and Kinetics of Vesicles Formation Processes. *Adv. Colloid Interface Sci.* **2010**, *161*, 77–88.
- (9) Discher, D. E.; Eisenberg, A. Polymer Vesicles. *Science* **2002**, *297*, 967–973.
- (10) Lasic, D. D. *Liposomes: From Physics to Applications*; Elsevier: Amsterdam, 1993.
- (11) Antonietti, M.; Förster, S. Vesicles and Liposomes: A Self-Assembly Principle Beyond Lipids. *Adv. Mater.* **2003**, *15*, 1323–1333.
- (12) Soussan, E.; Cassel, S.; Blanzat, M.; Rico-Lattes, I. Drug Delivery by Soft Matter: Matrix and Vesicular Carriers. *Angew. Chem., Int. Ed.* **2009**, *48*, 274–288.
- (13) Medvedeva, A. D.; Maslov, M. A.; Serikov, R. N.; Morozova, N. G.; Serebrennikova, G. A.; Sheglov, D. V.; Latyshev, A. V.; Vlassov, V. V.; Zenkova, M. A. Novel Cholesterol-Based Cationic Lipids for Gene Delivery. *J. Med. Chem.* **2009**, *52*, 6558–6568.
- (14) Guo, X.; Szoka, F. C., Jr. Chemical Approaches to Triggerable Lipid Vesicles for Drug and Gene Delivery. *Acc. Chem. Res.* **2003**, *36*, 335–341.
- (15) Zhi, D.; Zhang, S.; Cui, S.; Zhao, Y.; Wang, Y.; Zhao, D. The Headgroup Evolution of Cationic Lipids for Gene Delivery. *Bioconjugate Chem.* **2013**, *24*, 487–519.
- (16) Marianecchi, C.; Di Marzio, L.; Rinaldi, F.; Celia, C.; Paolino, D.; Alhaique, F.; Esposito, S.; Carafa, M. Niosomes from 80s to Present:

The State of the Art. *Adv. Colloid Interface Sci.* **2013**, DOI: 10.1016/j.cis.2013.11.018.

- (17) Waterhouse, D. N.; Tardi, P. G.; Mayer, L. D.; Bally, M. B. A Comparison of Liposomal Formulations of Doxorubicin with Drug Administered in Free Form: Changing Toxicity Profiles. *Drug Saf.* **2001**, *24*, 903–920.
- (18) Chang, H.-I.; Yeh, M.-K. Clinical Development of Liposome-Based Drugs: Formulation, Characterization, and Therapeutic Efficacy. *Int. J. Nanomed.* **2012**, *7*, 49–60.
- (19) Felnerova, D.; Viret, J. F.; Glück, R.; Moser, C. Liposomes and Virosomes as Delivery Systems for Antigens, Nucleic Acids and Drugs. *Curr. Opin. Biotechnol.* **2004**, *15*, 518–529.
- (20) Park, J. W. Liposome-Based Drug Delivery in Breast Cancer Treatment. *Breast Cancer Res.* **2002**, *4*, 95–99.
- (21) Dai, Y.; Zhou, R.; Liu, L.; Lu, Y.; Qi, J.; Wu, W. Liposomes Containing Bile Salts as Novel Ocular Delivery Systems for Tacrolimus (FK506): In Vitro Characterization and Improved Corneal Permeation. *Int. J. Nanomed.* **2013**, *8*, 1921–1933.
- (22) Immordino, M. L.; Dosio, F.; Cattel, L. Stealth Liposomes: Review of the Basic Science, Rationale, and Clinical Applications, Existing and Potential. *Int. J. Nanomed.* **2006**, *1*, 297–315.
- (23) Chen, C.; Han, D.; Cai, C.; Tang, X. An Overview of Liposome Lyophilization and Its Future Potential. *J. Controlled Release* **2010**, *142*, 299–311.
- (24) Du, J.; O'Reilly, R. K. Advances and Challenges in Smart and Functional Polymer Vesicles. *Soft Matter* **2009**, *5*, 3544–3561.
- (25) Yeagle, P. L. Modulation of Membrane Function by Cholesterol. *Biochimie* **1991**, *73*, 1303–1310.
- (26) Yeagle, P. L. Cholesterol and the Cell Membrane. *Biochim. Biophys. Acta* **1985**, *822*, 267–287.
- (27) Bloch, K. E. Sterol. Structure and Membrane Function. *Crit. Rev. Biochem. Mol. Biol.* **1983**, *14*, 47–92.
- (28) Hanukoglu, I. Steroidogenic Enzymes: Structure, Function, and Role in Regulation of Steroid Hormone Biosynthesis. *J. Steroid Biochem. Mol. Biol.* **1992**, *43*, 779–804.
- (29) Incardona, J. P.; Eaton, S. Cholesterol in Signal Transduction. *Curr. Opin. Cell Biol.* **2000**, *12*, 193–203.
- (30) Maxfield, F. R.; Tabas, I. Role of Cholesterol and Lipid Organization in Disease. *Nature* **2005**, *438*, 612–621.
- (31) Simons, K.; Ikonen, E. How Cells Handle Cholesterol. *Science* **2000**, *290*, 1721–1726.
- (32) Tulenko, T. N.; Chen, M.; Mason, P. E.; Mason, R. P. Physical Effects of Cholesterol on Arterial Smooth Muscle Membranes: Evidence of Immiscible Cholesterol Domains and Alterations in Bilayer Width during Atherogenesis. *J. Lipid Res.* **1998**, *39*, 947–956.
- (33) Davis, A. P. Cholaphanes et al.; Steroids as Structural Components in Molecular Engineering. *Chem. Soc. Rev.* **1993**, *22*, 243.
- (34) Bhattacharya, S.; Haldar, S. Interactions between Cholesterol and Lipids in Bilayer Membranes. Role of Lipid Headgroup and Hydrocarbon Chain-Backbone Linkage. *Biochim. Biophys. Acta* **2000**, *1467*, 39–53.
- (35) Svobodová, H.; Noponen, V.; Kolehmainen, E.; Sievänen, E. Recent Advances in Steroidal Supramolecular Gels. *RSC Adv.* **2012**, *2*, 4985–5007.
- (36) Dutta, S.; Kar, T.; Mandal, D.; Das, P. K. Structure and Properties of Cholesterol-based Hydrogelators with Varying Hydrophilic Terminals: Biocompatibility and Development of Antibacterial Soft Nanocomposites. *Langmuir* **2013**, *29*, 316–327.
- (37) Panzner, S.; Siepi, E.; Lutz, S.; Reinsch, C.; Muller, C. Transfection Enhancer Element-Containing Lipids and Lipid Assemblies for Transfection of Cells. *U.S. Pat. Appl. Publ.*, US 20080306153, Dec 11, 2008.
- (38) Goodwin, N. C.; Endert, G.; Herzog, N.; Kerwitz, Y.; Panzner, S.; Rodrigueza, W. Amphoteric Liposome Formulation for Delivery of DNAi Oligonucleotides for the Treatment of Cancer. *PCT Int. Appl.*, WO 2007064857, June 7, 2007.
- (39) Endert, G.; Kerwitz, Y.; Fellermeier, M. Serum-Stable Amphoteric Liposomes for the Delivery of Oligonucleotides. *PCT Int. Appl.*, WO 2005094783, Oct 13, 2005.

- (40) Oe, S.; Katsura, K.; Nagata, Y.; Arai, T.; Yamamoto, K. Preparation of Cholesterol Carbamate Derivatives. JP 04026699, Jan 29, 1992.
- (41) Ioffe, D. V.; Klimov, A. N.; Mal'tseva, O. A.; Nekrasova, V. B. Water-Soluble Sterol Derivatives. *Khim. Prir. Soedin.* **1980**, *5*, 655–657.
- (42) Rodriguez, W.; Goodwin, N. C. Amphoteric Liposome Formulations Containing Interfering DNA for Cancer Therapy. *PCT Int. Appl.*, WO 2009051712, Apr 23, 2009.
- (43) Panzner, S.; Endert, G.; Rauchhaus, U.; Herzog, N.; Muller, N. An Efficient Method for Loading Amphoteric Liposomes with Nucleic Acid Active Substances. *PCT Int. Appl.*, WO 2007107304, Sep 27, 2007.
- (44) Kunitake, T. Synthetic Bilayer Membranes: Molecular Design, Self-Organization, and Application. *Angew. Chem., Int. Ed. Engl.* **1992**, *32*, 709–726.
- (45) Kaler, E. W.; Murthy, A. K.; Rodriguez, B. E.; Zasadzinski, J. A. Spontaneous Vesicle Formation in Aqueous Mixtures of Single-Tailed Surfactants. *Science* **1989**, *245*, 1371–1374.
- (46) Huang, J.-B.; Zhu, B.-Y.; Zhao, G.-X.; Zhang, Z.-Y. Vesicle Formation of a 1:1 Catanionic Surfactant Mixture in Ethanol Solution. *Langmuir* **1997**, *13*, 5759–5761.
- (47) Junyaprasert, V. P.; Singhsa, P.; Suksiriworapong, J.; Chantasart, D. Physicochemical Properties and Skin Permeation of Span 60/Tween 60 Niosomes of Ellagic Acid. *Int. J. Pharm.* **2012**, *423*, 303–311.
- (48) Ghosh, S.; Dey, J. Interaction of Sodium *N*-Lauroylsarcosinate with *N*-Alkylpyridinium Chloride Surfactants: Spontaneous Formation of pH-Responsive, Stable Vesicles in Aqueous Mixtures. *J. Colloid Interface Sci.* **2011**, *358*, 208–216.
- (49) Di Marzio, L.; Marianecchi, C.; Petrone, M.; Rinaldi, F.; Carafa, M. Novel pH-Sensitive Non-ionic Surfactant Vesicles: Comparison between Tween 21 and Tween 20. *Colloids Surf., B* **2011**, *82*, 18–24.
- (50) Mukhopadhyay, S.; Maitra, U. Chemistry and Biology of Bile Acids. *Curr. Sci.* **2004**, *87*, 1666–1683.
- (51) Small, D. M. In *The Bile Salts*; Nair, P. P., Kritchevsky, D., Eds.; Plenum Press: New York, 1971; Vol. 1.
- (52) Kim, T. H.; Kwona, N. Y.; Lee, T. S. Synthesis of Organogelling, Fluoride Ion-Responsive, Cholesteryl-Based Benzoxazole Containing Intra- and Intermolecular Hydrogen-Bonding Sites. *Tetrahedron Lett.* **2010**, *51*, 5596–5600.
- (53) Debye, P. *Polar Molecules*; Dover: New York, 1929.
- (54) Roy, S.; Mohanty, A.; Dey, J. Microviscosity of Bilayer membranes of Some *N*-Acylamino Acid Surfactants Determined by Fluorescence Probe Method. *Chem. Phys. Lett.* **2005**, *414*, 23–27.
- (55) Lakowicz, J. R. *Principles of Fluorescence Spectroscopy*; Plenum Press: New York, 1983.
- (56) Shinitzky, M.; Barenholz, Y. Dynamics of the Hydrocarbon Layer in Liposomes of Lecithin and Sphingomyelin Containing Dicetylphosphate. *J. Biol. Chem.* **1974**, *249*, 2652–2657.
- (57) Roy, S.; Dey, J. Spontaneously Formed Vesicles of Sodium *N*-(11-Acrylamidoundecanoyl)-glycinate and *L*-Alaninate in Water. *Langmuir* **2005**, *21*, 10362–10369.
- (58) He, F.; Xu, G.; Pang, J.; Ao, M.; Han, T.; Gong, H. Effect of Amino Acids on Aggregation Behaviors of Sodium Deoxycholate at Air/Water Surface: Surface Tension and Oscillating Bubble Studies. *Langmuir* **2011**, *27*, 538–545.
- (59) Rosen, M. J. *Surfactants and Interfacial Phenomena*, 3rd ed.; Wiley-Interscience: New York, 2004; pp 60–64.
- (60) Israelachvili, J. N.; Mitchell, D. J.; Ninham, B. W. Theory of Self-Assembly of Hydrocarbon Amphiphiles into Micelles and Bilayers. *J. Chem. Soc., Faraday Trans. 2* **1976**, *72*, 1525–1568.
- (61) Calculated using ACD/Labs software v11.02 (© 1994–2013 ACD/Labs) by SciFinder.
- (62) Saitoh, T.; Taguchi, K.; Hiraide, M. Evaluation of Hydrophobic Properties of Sodium Dodecylsulfate/ γ -Alumina Admicelles Based on Fluorescence Spectra of *N*-Phenyl-1-Naphthylamine. *Anal. Chim. Acta* **2002**, *454*, 203–208.
- (63) Chapman, C. F.; Fee, R. S.; Maroncelli, M. Measurements of the Solute Dependence of Solvation Dynamics in *l*-Propanol: The Role of Specific Hydrogen-Bonding Interactions. *J. Phys. Chem.* **1995**, *99*, 4811–4819.
- (64) Horng, M. L.; Gardecki, J. A.; Papazyan, A.; Maroncelli, M. Subpicosecond Measurements of Polar Solvation Dynamics: Coumarin 153 Revisited. *J. Phys. Chem.* **1995**, *99*, 17311–17337.
- (65) Kalyanasundaram, K.; Thomas, J. K. Environmental Effects on Vibronic Band Intensities in Pyrene Monomer Fluorescence and Their Application in Studies of Micellar Systems. *J. Am. Chem. Soc.* **1977**, *99*, 2039–2044.
- (66) Birks, J. B. *Photophysics of Aromatic Molecules*; Wiley-Interscience: New York, 1970; Section 4.
- (67) Vethamuthu, M. S.; Almgren, M.; Mukhtar, E.; Bahadur, P. Fluorescence Quenching Studies of the Aggregation Behavior of the Mixed Micelles of Bile Salts and Cetyltrimethylammonium Halides. *Langmuir* **1992**, *8*, 2396–2404.
- (68) Ueno, M.; Kimoto, Y.; Ikeda, Y.; Momose, H.; Zana, R. Study on the Aggregation Number of Mixed Micelles in Aqueous Binary Mixtures of the Bile Salts and Nonionic Surfactant. *J. Colloid Interface Sci.* **1987**, *117*, 179–186.
- (69) Shinitzky, M.; Dianoux, A.-C.; Gitler, C.; Weberil, G. Microviscosity and Order in the Hydrocarbon Region of Micelles and Membranes Determined with Fluorescent Probes. I. Synthetic Micelles. *Biochemistry* **1971**, *10*, 2106–2113.
- (70) Shinitzky, M.; Yuli, I. Lipid Fluidity at the Submacroscopic Level: Determination by Fluorescence Polarization. *Chem. Phys. Lipids* **1982**, *30*, 261–282.
- (71) Zana, R.; Martin, I.; Lévy, H. Alkanediyl- α,ω -bis-(dimethylalkylammonium bromide). 7. Fluorescence Probing Studies of Micelle Micropolarity and Microviscosity. *Langmuir* **1997**, *13*, 5552–5557.
- (72) Caracciolo, G.; Pozzi, D.; Caminiti, R.; Marianecchi, C.; Moglioni, S.; Carafa, M.; Amenitsch, H. Effect of Hydration on the Structure of Solid-Supported Niosomal Membranes Investigated by in situ Energy Dispersive X-ray Diffraction. *Chem. Phys. Lett.* **2008**, *462*, 307–312.
- (73) Pozzi, D.; Caminiti, R.; Marianecchi, C.; Carafa, M.; Santucci, E.; De Sanctis, S. C.; Caracciolo, G. Effect of Cholesterol on the Formation and Hydration Behavior of Solid-Supported Niosomal Membranes. *Langmuir* **2010**, *26*, 2268–2273.
- (74) Waugh, A.; Grant, A. *Anatomy and Physiology in Health and Illness*, 9th ed.; Churchill Livingstone: Edinburgh, Scotland, 2001; p 22.
- (75) Peters, T. *All About Albumin: Biochemistry, Genetics, and Medical Applications*; Academic: San Diego, 1996.
- (76) Anand, U.; Jash, C.; Mukherjee, S. Spectroscopic Probing of the Microenvironment in a Protein-Surfactant Assembly. *J. Phys. Chem. B* **2010**, *114*, 15839–15845.
- (77) Roda, A.; Cappelleri, G.; Aldini, R.; Barbara, L. Quantitative Aspects of the Interaction of Bile Acids with Human Serum Albumin. *J. Lipid Res.* **1982**, *23*, 490–495.
- (78) Pico, G. A.; Houssier, C. Bile Salts-Bovine Serum Albumin Binding: Spectroscopic and Thermodynamic Studies. *Biochim. Biophys. Acta* **1989**, *999*, 128–134.